

Unshielded Operation of a Miniaturized Radiofrequency Magnetometer in Earth's Field

John Dhombridge^{1,2}, Neil Claussent¹, Tomas Iivanainen¹, and Peter Schwindt^{1,2}

¹Sandia National Laboratories, Albuquerque, New Mexico, United States.

²Center for Quantum Information and Control, Dept. of Physics & Astronomy, University of New Mexico, Albuquerque, New Mexico United States

Project Goal

- Development of a fieldable optically pumped magnetometer (OPM) capable of operating with high sensitivity unshielded in Earth's field.

Our Approach

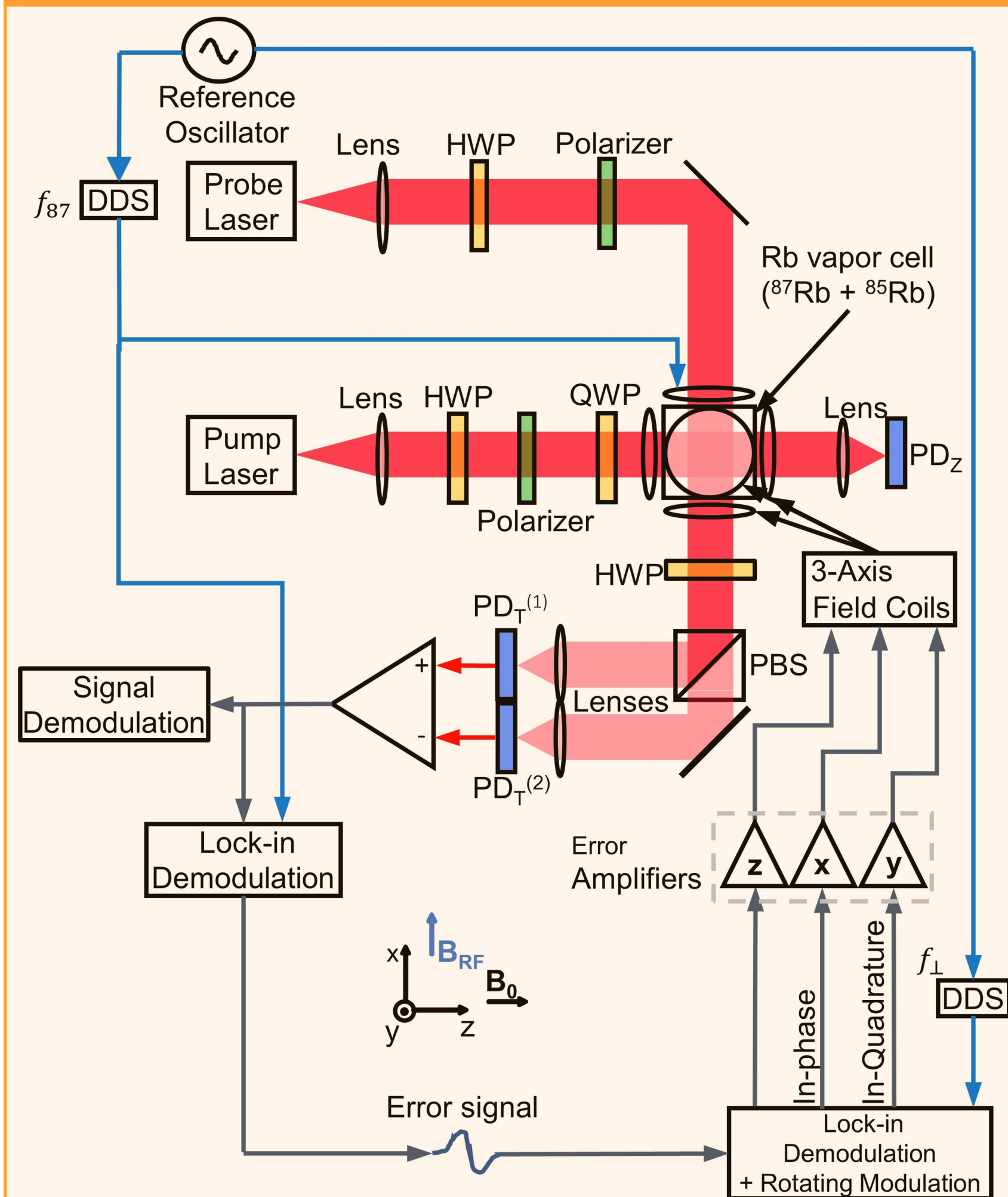


Fig. 1: Layout of our magnetometer at a high level, showing lasers, optics, and electronics. DDS: direct digital synthesizer. HWP: half-wave plate. QWP: quarter wave plate. PBS: polarizing beam-splitter. PD_z: z axis photodiode. PD_T(1,2): transverse photodiodes 1 and 2. The difference signal of the transverse photodiodes is used for balanced photodetection after transimpedance amplification

- We use both isotopes in natural abundance Rubidium vapor (27.8% ⁸⁷Rb and 72.2% ⁸⁵Rb) to create a comagnetometer within a single vapor cell.
 - ⁸⁵Rb for radiofrequency (RF) magnetometer using the tuned resonance approach of Savukov et al. [1]
 - ⁸⁷Rb for OPM *variometer* based on the approach of Alexandrov et al. [2]
- RF magnetometer is resonantly driven Larmor precession of longitudinally polarized atoms (Figure 1)
 - Longitudinal field $B_0 = \frac{2\pi}{\gamma_{85}} f_{RF}$ is applied along the z axis
 - $\gamma_{85} = 4.67 \text{ Hz/nT}$
 - f_{RF} is the sensing frequency.
 - Pump laser longitudinally polarizes spin S along optical (z) axis.
 - An external RF field polarized in the transverse (xy) plane drives resonant Larmor precession.
- Variometer signal used to derive feedback to stabilize low frequency ($\leq 60 \text{ Hz}$) field for RF magnetometer operation.
 - ⁸⁷Rb driven at 3/2 RF frequency of ⁸⁵Rb gives total error signal for feedback to $|B| = \sqrt{B_z^2 + B_x^2 + B_y^2}$
 - Rotating modulation gives transverse error signals for feedback to B_x, B_y . (Figure 3)
 - Combined signals give three axis field control

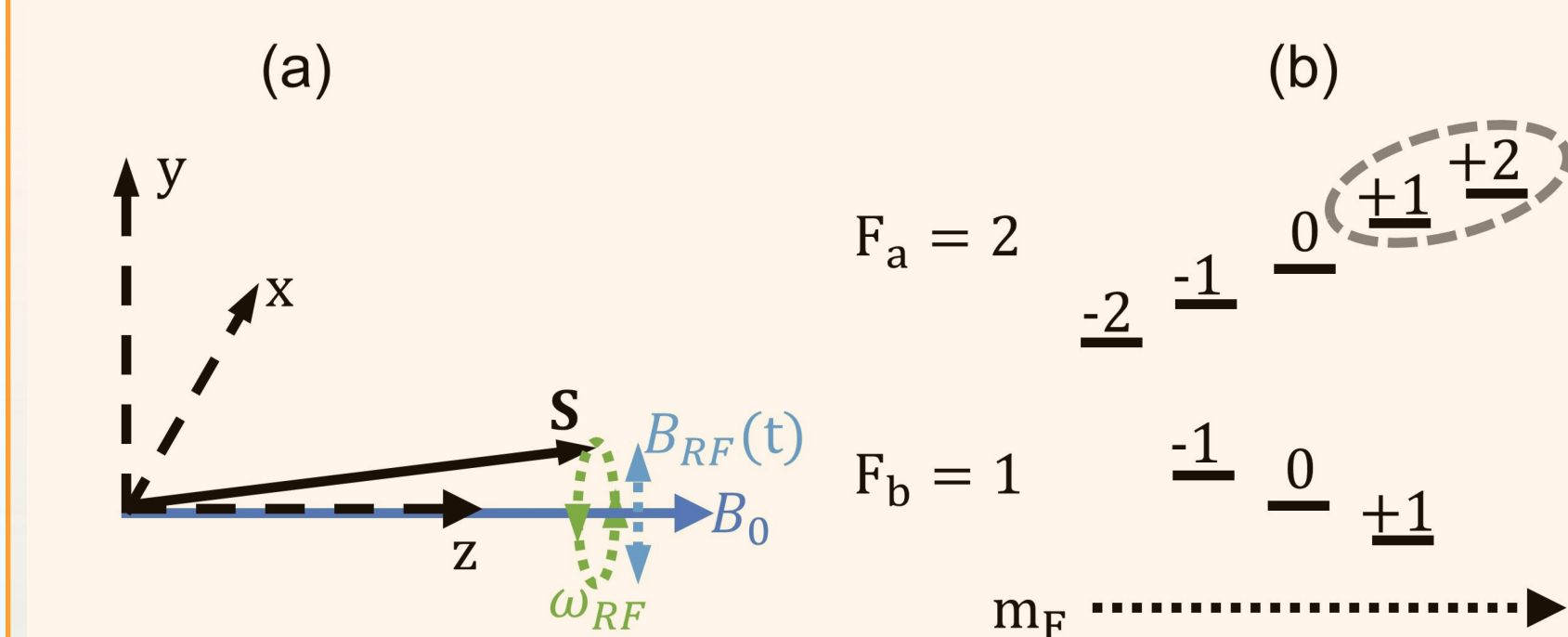


Fig. 2: The principle of an RF OPM. (a) RF magnetic field $B_{RF}(t)$ drives resonant precession of Atomic Spin S about the longitudinal axis at frequency ω_{RF} . (b), level diagram of an $I = 3/2$ alkali atom, highlighting the stretched state levels that are resonantly driven.

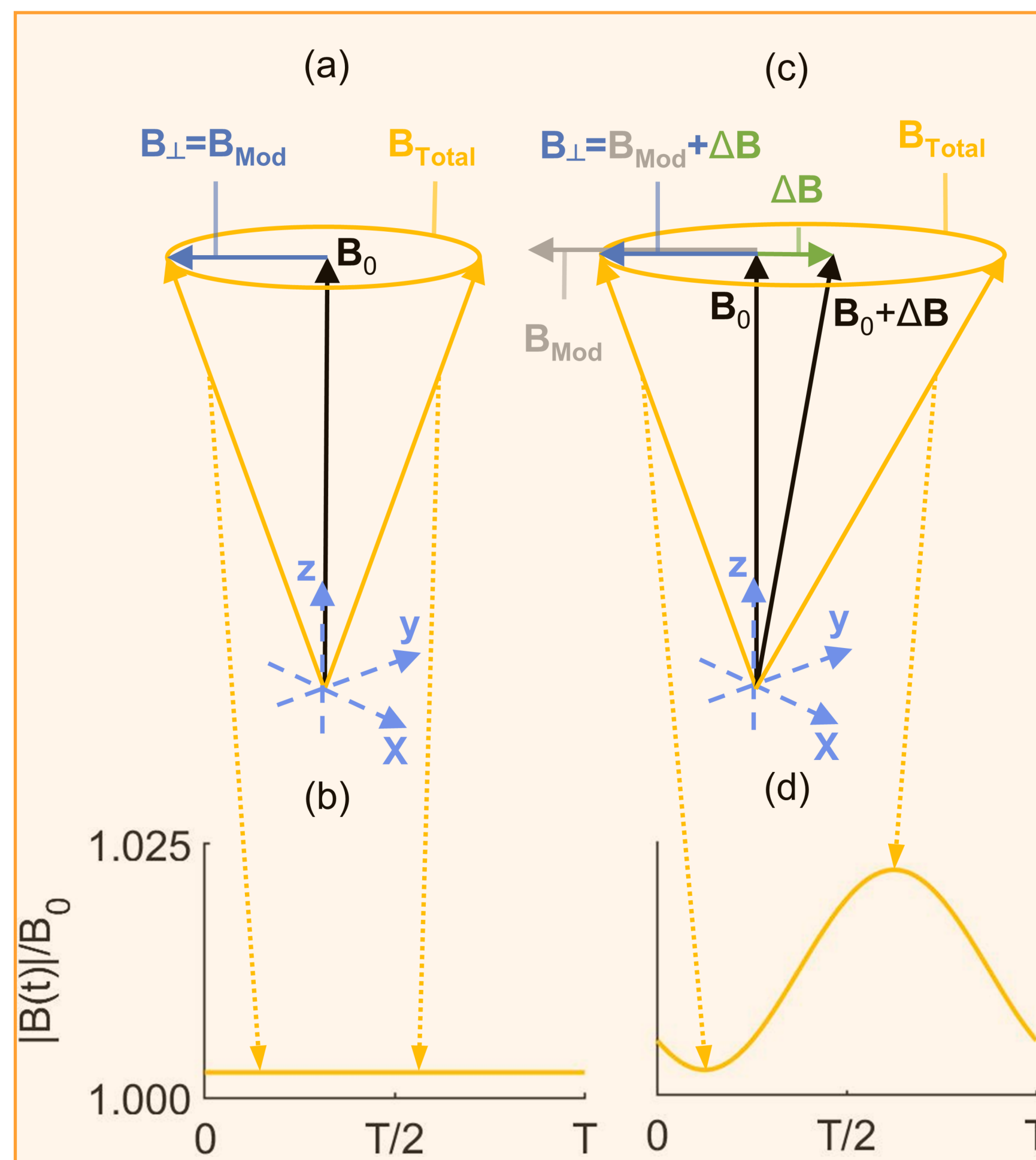


Fig. 3: Dynamics of a variometer. (a) Rotating modulation is added in the transverse plane. The total field amplitude $|B(t)| = \sqrt{B_0^2 + B_{\perp}^2}$ remains constant, as shown in (b). In (c), an offset ΔB in the transverse plane causes a periodic modulation of the total field amplitude at frequency $1/T$ as shown in (d).

Miniaturization

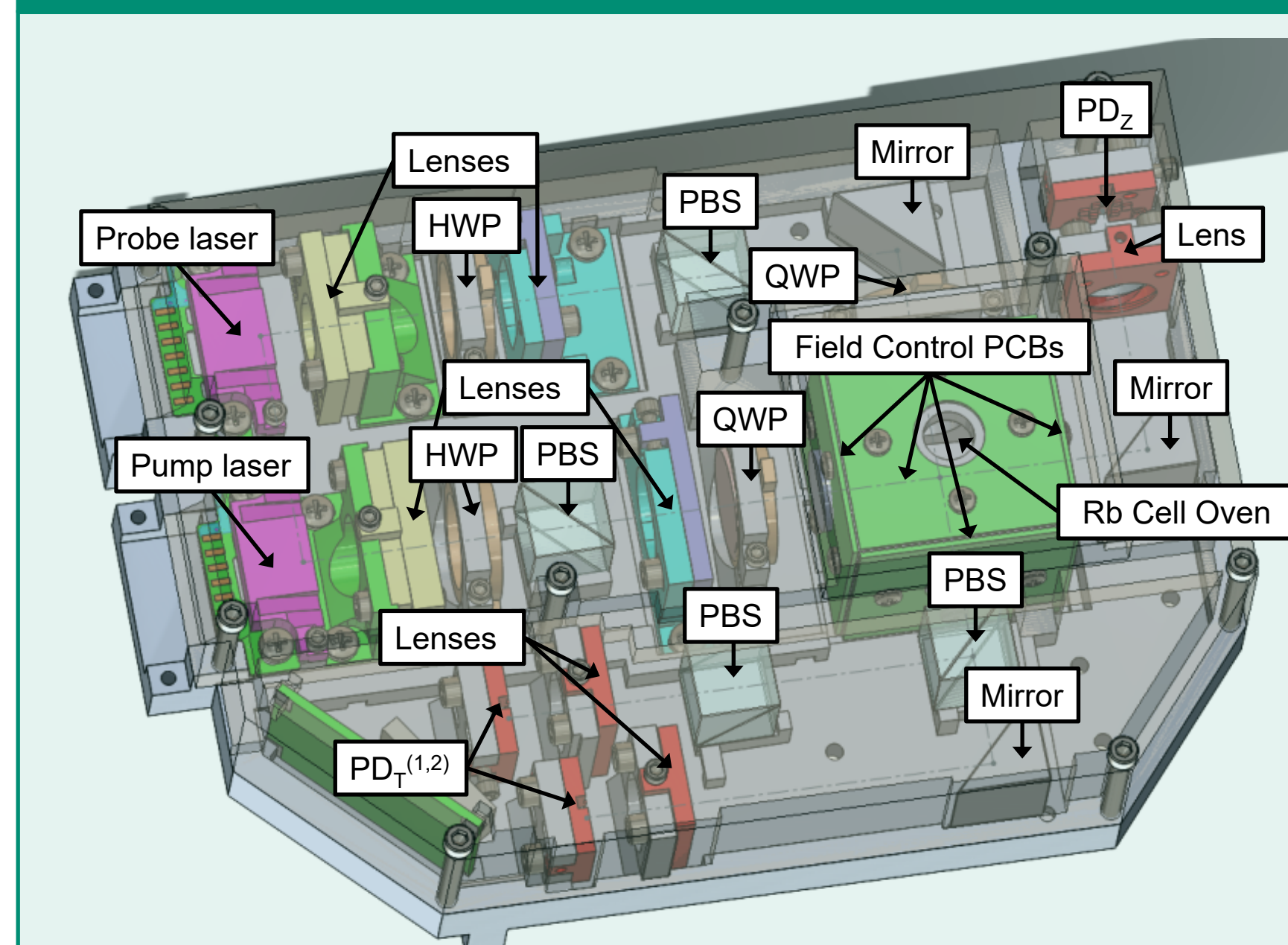


Figure 4: SolidWorks model of the 3D printed miniaturized magnetometer. Labels correspond to Figure 1.

- Optical layout via Zemax opticstudio.
- Miniaturized CAD design in SolidWorks.
- Final design 3D printed from ABS plastic and Ultem (for cell heater).
 - $< 600 \text{ cm}^3$ total volume.
- Miniaturized field control coils printed on 6-layer PCBs
 - Current distributions over all six faces from bfieldtools [3].
 - Current distributions implemented via 3 layer printed circuit boards (PCBs).
 - PCBs connected via twisted pair wires.

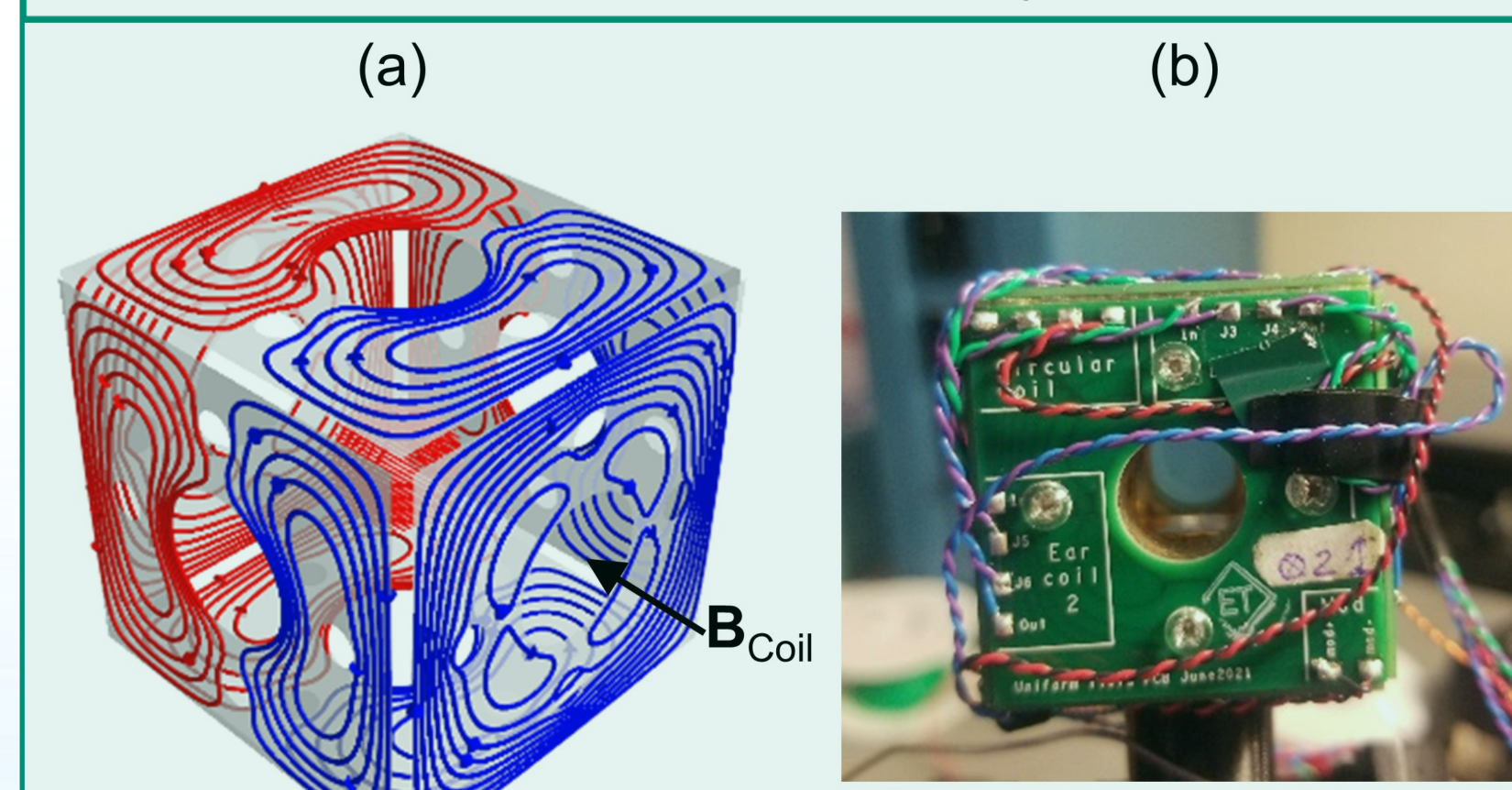


Fig. 5: Details of the field control PCBs. (a) Current distribution over all six faces of the cubic vapor cell oven. (b) PCBs mounted on the cell oven and connected with twisted pair wires

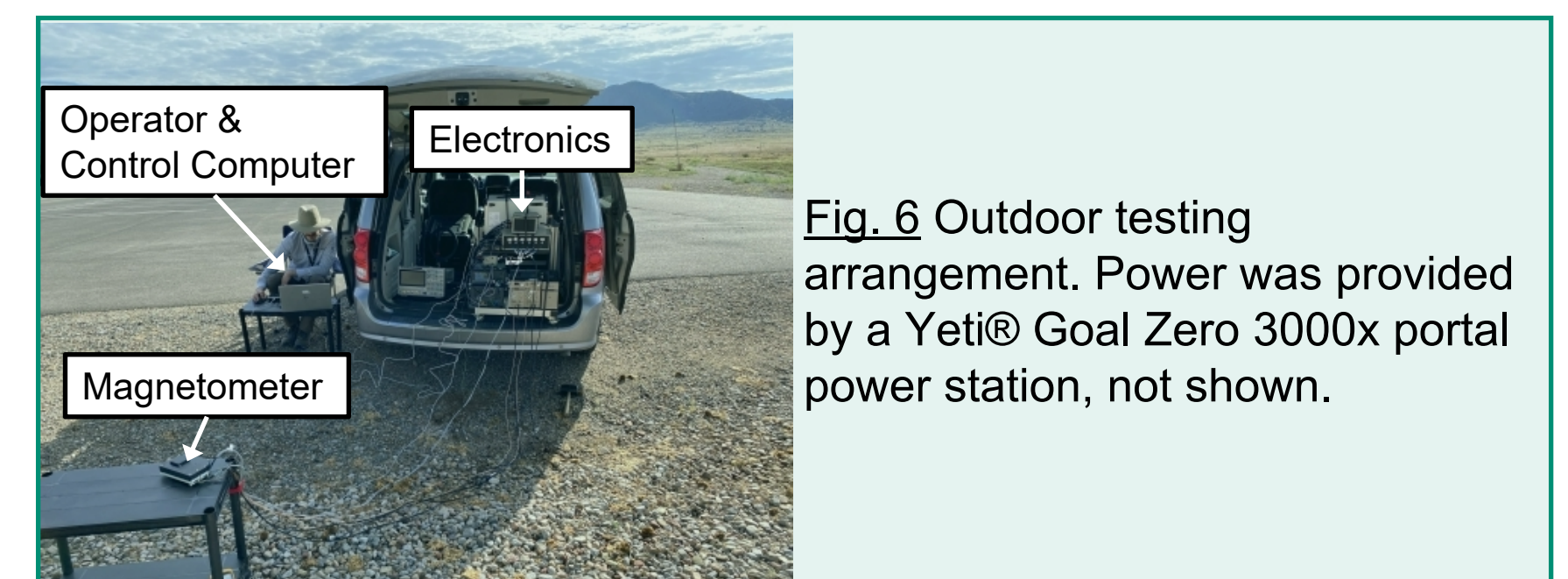


Fig. 6 Outdoor testing arrangement. Power was provided by a Yeti® Goal Zero 3000x portal power station, not shown.

Feedback Performance

Channel	Bandwidth (Hz)	Max Slew Rate ($\mu\text{T/s}$)
z	97	33
x	67	8
y	60	8

Table 1: Feedback performance of the variometer after PID optimization. Bandwidths were extracted from fitting decaying exponentials to the feedback response of the system to a square wave modulation of the magnetic field. Slew rates were found by applying a 1s linear ramp of the magnetic field and increasing the amplitude until the system became unstable.

RF Sensitivity

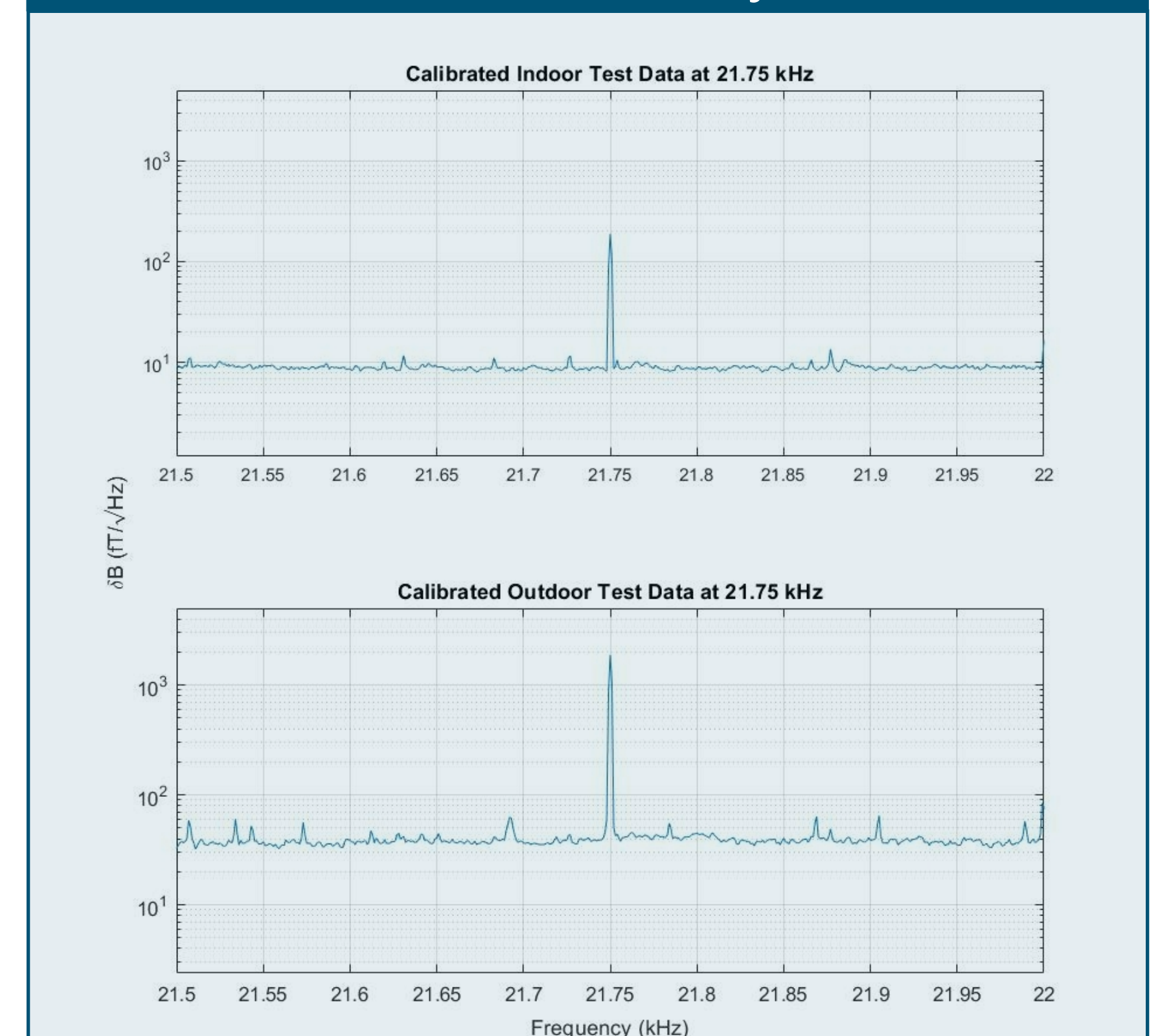


Fig. 7: Amplitude spectral density data showing the RF sensitivity of the system in $\text{fT}/\sqrt{\text{Hz}}$, both in the lab within an aluminum shield to limit high frequency noise (above), and completely unshielded outdoors (below). Here we see that the fundamental noise floor is below $10 \text{ fT}/\sqrt{\text{Hz}}$, while the noise floor outdoors is just above $40 \text{ fT}/\sqrt{\text{Hz}}$, indicating the noise floor seen outdoors is due to true magnetic noise that is present in the unshielded spectrum at these frequencies.

Acknowledgements

- Thanks to Jeffrey Bach for sharing his knowledge of various aspects of RF engineering and signal processing, and lending test equipment.
- Thanks to Lee Marshall for his help with design and development of the system electronics.

References

- I. M. Savukov, S. J. Seltzer, M. V. Romalis, and K. L. Sauer, Tunable atomic magnetometer for detection of radio-frequency magnetic fields, *Phys. Rev. Lett.* 95,063004 (2005).
- E. B. Alexandrov, M. Balabas, V. N. Kulyasov, A. E. Ivanov, A. S. Pazzgalev, J. L. Rasson, A. K. Vershovski, and N. N. Yakobson, Three-component variometer based on a scalar potassium sensor, *Measurement Science and Technology* 15, 918 (2004).
- R. Zetter, A. J. M'akinen, J. Iivanainen, K. C. J. Zevenhoven, R. J. Ilmonemi, and L. Parkkonen, Magnetic field modeling with surface currents. part ii. Implementation and usage of bfieldtools, *Journal of Applied Physics* 128, 063905 (2020), <https://doi.org/10.1063/5.0016087>.